A report on the MECS misalignments and the MECS positioning capabilities

MECS Report MECS_OFC_4
Issue 1 - 02/09/97

prepared by L.Chiappetti - IFCTR

1 Introduction

1.1 Executive summary

The purpose of this report is the determination of the misalignments between the MECS detector reference system and the SAX spacecraft reference system.. Once the misalignments are known, they can be used in conjunction with the satellite attitude to convert detector coordinates to and from celestial coordinates (i.e. to measure a source position on the sky from its pixel position, or to predict where a known celestial source falls on a detector image).
An additional purpose of this report is to assess the error budget for source positioning, giving a breakdown into its various components (due to the measurement of pixel positions, to the attitude and to the errors in the misalignments).

The misalignments have been determined analysing the LMC X-3 raster scans (and verifying the results on the Cyg X-1 raster). The direction of the pointing (**Z**) axis of the detectors is offset by about 10 arcmin in one direction and by a quantity between 0.5 and 2.5 arcmin (according to detector unit) in the other direction. The typical uncertainty on such values is of the order of 0.25 arcmin. There is no evidence of rotation around the **Z** axis within an uncertainty of a couple of degrees.
The scatter on the celestial position (reconstructed using the determined misalignments) for both datasets of LMC X-3 and Cyg X-1 is within 15-20 arcsec. The same extent is shown by a numeric simulation.

The determination of the uncertainties on attitude and centroid measurements is outside of the scope of the present report. In the best case (attitude known within a few arcsec, centroid known at least at 0.3 detector pixels) the total error is dominated by the misalignments. In the worst case one can combine quadratically the errors (e.g. an huge attitude uncertainty of 30 arcsec, and a centroid error of more than one pixel gives a total uncertainty of the order of one arcmin).

The misalignments are defined in the remainder of section 1, the data are presented in section 2, while section 3 describes the preliminary data reduction, and section 4 describes the misalignment analysis. The results on the misalignments are presented in section 5, while section 6 describes the error budgets. Finally appendix A summarizes the mathematical notation used.

1.2 Definitions

We first give the definition of the misalignments. It is known from the ground calibrations that the electronics axes (measuring *x y* of events) are aligned with the detector physical axes (given by the strongback structure supporting the entrance Be window). It is also known that each couple of detectors is mounted with the respective optics on a carbon fiber optical bench. The alignment with the satellite has been performed in such a way that detector M3 has its *x y* axes grossly parallel to the spacecraft **XY** axes, while detectors M1 and M2 have their *x y* axes flipped with respect to the spacecraft axes (i.e. *x* // -**X** and *y* // -**Y**). The Z axis of the detector-optics system, and of the satellite, are those defining the respective pointing direction.

If we call **XYZ** the spacecraft axes and *xyz* the detector axes, we can describe their respective misalignments via 3 angles α,β,γ. These angles have customarily been defined as follows (e.g. Gronenschild 1985, *Exosat Express* **12**, 53) and are illustrated in Fig. 1a-d.

> First, one applies a rotation of an angle α around the **Z** axis (this brings **XYZ** into *x'y'z'* leaving the detector plane alone; see fig. 1a).

Second, one applies a rotation of an angle β around the *y'* axis (this brings *x'y'z'* into *x"y"z"*, tilting the detector plane; see fig. 1b)
Finally one applies a third rotation of an angle γ around the *x"* axis (this brings *x"y"z"* into the final *xyz* system with a further tilt of the detector plane; see fig. 1c)
Fig. 1d summarizes the effect of the cumulative rotation from **XYZ** to *xyz*.

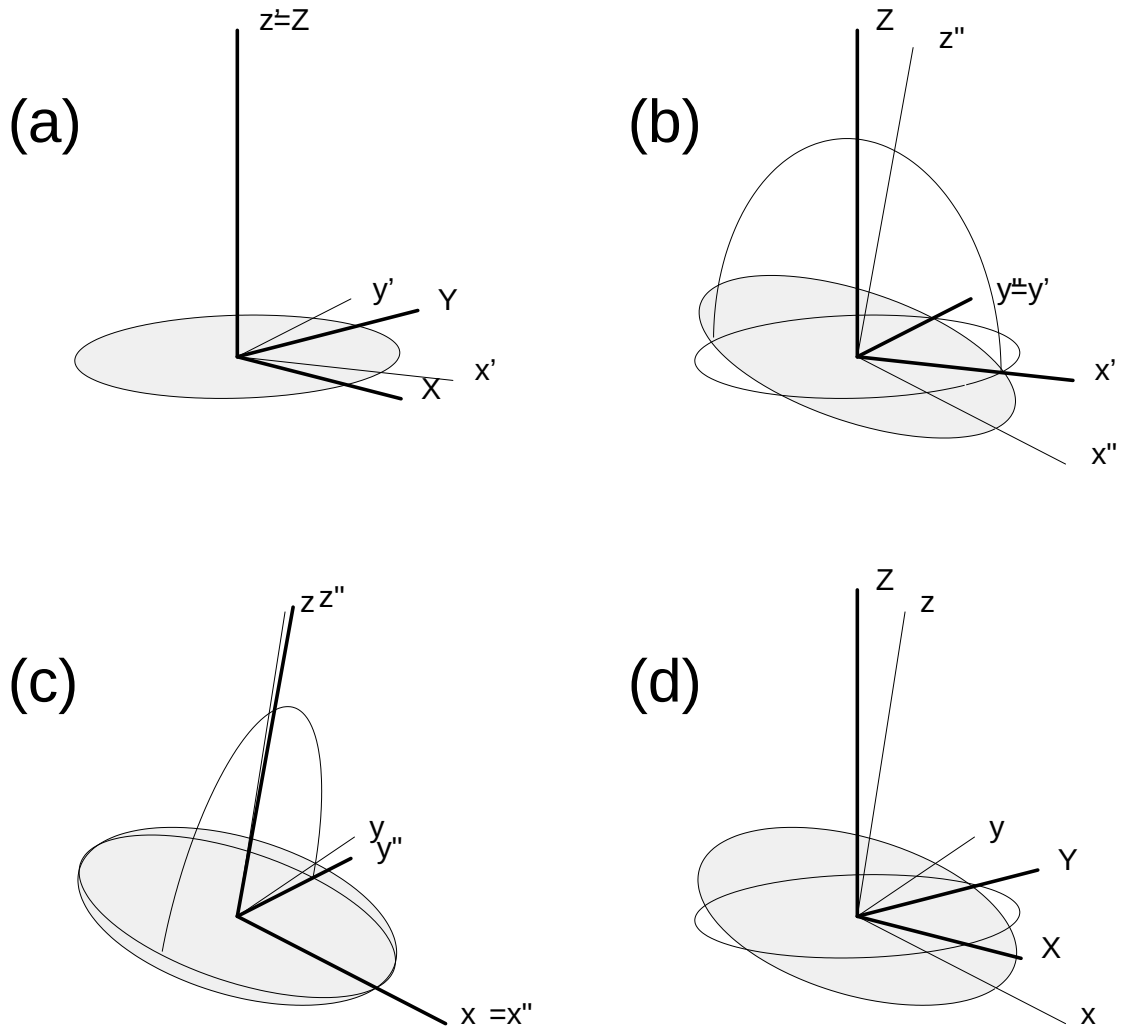

Fig. 1 Each panel shows the rotation from the thick axis system to the thin axis system, namely: (a) rotation of α around the Z axis ; (b) rotation of β around the y' axis ; (c) rotation of γ around the x axis ; (d) combination of the three rotations. In each panel the gray circle indicates the detector plane after the rotation. The orientation of the axes it the one for M3. The rotation angles are also those for M3, exaggerated by a factor 100.

2 The MECS rasters

The typical way to measure detector-to-satellite misalignments is to perform a raster scan, pointing the same target at different, known attitudes. One can then use the measured detector position together with the knowledge of the attitude and of the target celestial position to determine the misalignments. We list below the raster scans performed with BeppoSAX during the SVP.

2.1 The first LMC X-3 raster

A raster on LMC X-3 was originally planned for the very purpose of misalignment determination. It should have included : one on-axis pointing, a cross of four near-axis pointing in the vertical and horizontal direction, a cross of four near-axis pointing in the diagonal directions, and four further off-axis pointings in the diagonal directions (45 and 22.5 degrees from the axes). For contingency reasons the on-axis and the first three near-axis pointings were not performed.
This raster therefore consists of 9 consecutive OPs (even numbers from 1148 to 1164) done on 24-25 Oct 1996. The position of the relevant pointings are shown as asterisks on fig. 2a.
Note that two of the outermost points are close to the built-in calibration sources (and to the relevant avoidance region).

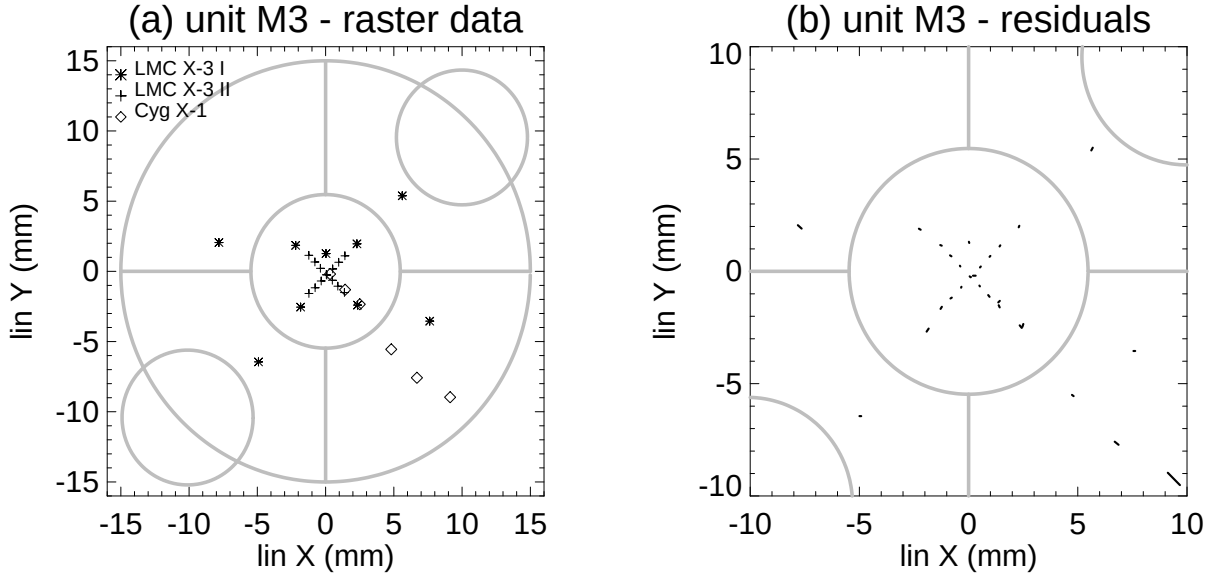

Fig. 2 raster scan data for unit M3 are shown (the data for units M1 and M2 are similar, only they are flipped left-to-right and top-to-bottom).
Panel (a) shows the measured centroid positions in mm on the detector plane. Different symbols indicate the two LMC X-3 rasters and the Cyg X-1 raster. The gray lines indicate the obstructions of the field of view due to the Be window edge, to the strongback structure, and to the calibration source holders.
Panel (b) is an enlargement of the central part of the field of view, and shows (as vectors) the residuals in mm of the positions computed from the attitude and the misalignments w.r.t. the measured positions.

2.2 The second LMC X-3 raster

A further raster on LMC X-3 was done on 27-28 Nov 1996 with the purpose of mapping the strongback grid of the LECS. It consists of two diagonal scans in the central region of the field of view (two on-axis pointings nearly overlapping). These data can be used to complement the first raster.
The dataset consists of 14 OPs (even numbers from 1306 to 1332.). The position of the relevant pointings are shown as crosses on fig. 2a.

2.3 The Cyg X-1 raster

A small raster of 6 pointings on Cyg X-1 was done on 12-13 Sep 96 with the purpose of studying the off-axis PSF and vignetting (see Conti *et al*. SPIE Conf. **3113** in press). The pointings were arranged on a single diagonal from the on-axis position up to the very edge of the field of view.
The dataset consists of 6 OPs (odd numbers from 903 to 913) and has been used for verification of the results obtained from the LMC X-3 rasters. The position of the relevant pointings are shown as diamonds on fig. 2a. (The innermost 3 points cover the same range of the LMC X-3 rasters.)

Note that the outermost point is on the very edge of the detector (watch for this when considering residuals).

2.4 The Crab raster

A further raster was performed on the Crab Nebula (OP 1049 to 1063) with the purpose of verification of the vignetting and of the off-field-of-view contamination (see also Conti *et al*. SPIE Conf. **3113** in press). These data have not been used here since the Crab is not a point source.

3 Data reduction

We summarize here the main steps of data reduction. Full details are kept in journal files (named `Journal`) in directories `~lucio/sax/PV/LMCX3/RasterI` and `RasterII` and `~lucio/sax/PV/CygX1/Raster`. The same directories contain also reduced data and the software used (mostly old or wrong versions). The final data and software for the combined analysis is in `~lucio/sax/PV/LMCX3/Rasters.` The analysis has been performed starting from the CDs containing data cleaned for spurious packet presence.

3.1 Filtering in attitude

The main point is that, in order to measure the misalignments, one needs to restrict oneself to intervals of *extremely* stable attitude (see also discussion in section 6.2).
We have preliminarily run the standard `saxauxcalc` program, and determined no-occultation time windows using both the `pointtype` flag and the `earth` angle greater than 3 degrees. We have compared the time window thus determined with the occultation of the source as shown by a time profile of scientific data, and concluded that the condition based on the Earth angle is cleaner particularly in the case of nearly-circumpolar sources like LMC X-3 (δ about -64 deg).
We have also generated the time windows corresponding to at least two star trackers in operation (using the `strconf` flag) and preliminarily restricted the analysis to the intersection of such window with the no occultation one.

However we have found that the attitude time profiles show erratic features (spikes and jumps) which are not always in correspondence with star tracker transitions. In some cases it is actually difficult to tell, from the visual inspection of attitude time profiles, which is the good interval to use. We have therefore proceeded to a different kind of filtering, based on positions *as observed by the MECS itself.*

3.2 Filtering in xy

We have therefore accumulated (using program `saxzaccum`) the time profiles of the mean (linearized) *x* and *y* position. The accumulation is restricted via a region file to the Be window (excluding the calibration sources) in order to take the mean *target* position. A further restriction in a ±45 pixel box (0.15 mm pixels used throughout) around the centroid allows to keep the error bars smaller (note that the mean position is a rough, quick-and-dirty estimator and does not imply any knowledge of - or fit on - the PSF or LSF).
We have then performed iteratively what follows :

Smoothed the *x* and *y* time profiles
Taken the mean and standard deviation of the smoothed time profile
Generate time windows where *x* and *y* are inside 2 standard deviations from the mean
Re-accumulated *x* and *y* time profiles in such time window
Repeated the above

The procedure has been terminated either when the standard deviation was less than 0.3 pixels (i.e. ~5 arcsec), or whenever the procedure converged and. no further improvement was possible (this occurred for some of the LMC X-3 points with a standard deviation of 0.4-0.5 pixels at least on one axis).

We have then conservatively excluded 30 sec on either side of each of the last time windows, and used these as intervals of stable attitude.We have performed all further accumulations in these time windows. Visual inspection was used to verify that stable attitude was achieved.

In particular we have accumulated the time profile of the six attitude parameters (i.e. the celestial coordinates α,δ of the spacecraft **X**,**Y**,**Z** axes, see appendix A.2) and taken the mean of such time profiles as the *reference attitude*.

3.3 Centroid in unlinearized coordinates

In a first instance (to avoid side effects due to the arbitrary choice of the linearized pixel size) we have measured the target position as follows :

> We have first accumulated an unlinearized image (in the stable attitude window).
> We have taken the pixel position as the centroid (barycentre) in a 50 pixel box in unlinearized coordinates.
> We have converted into mm from detector centre (i.e. linearized) such individual coordinate *x,y* using the standard linearization formulae [(20) and (21) in appendix A.10.i] for a fixed energy of 3.5 keV (we have verified from a mean spectrum that this is reasonable, the mean energy of an LMC X-3 spectrum is in fact 3.44 keV (and 4.04 keV for Cyg X-1).

Since no region selection was applied, the centroids of the positions closer to the calibration sources might be contaminated by the calibration sources (pulled on the outside). This has been cured restricting the centroid box.

3.4 Centroid in linearized coordinates

In a second instance we have instead used as target position the following :

> We have accumulated a linearized image (in the stable attitude window).
> We have taken the centroid (barycentre) in linearized pixels.
> We have converted such pixels into mm from detector centre using the appropriate formulae [(24) and (25) in appendix A.10.iii]

This way we average out any energy dependency, and we likely generate a cleaner PSF for the off-axis pointings. This is also closer to the standard user reduction. However since we apply a standard region selection, the calibration source avoidance region may cut out the outermost part of the PSF for pointings close to the calibration sources.

We have found no great difference between the two methods. Anyhow the final analysis *is based on linearized image centroids*.

Note that for both methods there is an equal bias for the determination of the "position" of off-axis sources. The centroid does not imply any model fitting to the PSF or LSF, but is the barycentre of the actual photon distribution. For off-axis sources there are significant wings of the PSF, and such position is usually pulled towards the centre of the detector with respect to the centre of the "ellipsoidal core" of the PSF.

4 Determination of misalignments

The starting point for the final misalignment analysis are therefore the following :

> a file with 3 couples per OP (one per MECS unit) of *xy* target positions (mm from detector centre)
> a file with the average attitude : the α,δ coordinates of the spacecraft **X**,**Y**,**Z** axes (6 numbers per OP, note that they are not all independent, three angles like α_Z , δ_Z and the roll ρ will suffice and are usually computed internally to the programs)
> the nominal target coordinates α_T ,δ_T

The nominal target coordinates are those reported by W3Browse/SIMBAD, and namely :

Target	RA α_T	Dec δ_T
LMC X-3	84.7350000	-64.0837222
Cyg X-1	299.5904160	+35.2016388

4.1 Trial and error method

From the attitude one can compute the Euler matrix [formulae (5) and (4)]; one can then guess the three misalignment angles α,β,γ and compute the product of the relevant rotation matrices ; one then computes the rotated Euler matrix with formula (8), derives from these on one hand the detector attitude (in particular the roll) with formula (28), on the other hand, using the target coordinates, one computes the gnomonic coordinates, corrects them for roll, and uses the platescale to pass from angular values to mm, using formulae (9) to (15). The results can be compared with measured mm coordinates.

One can then adjust by trial and error the α,β,γ angles until a satisfactory agreement is reached. One way to assess the agreement is to compute the residuals in mm between the predicted and measured coordinates, and to plot them as vectors (an example is shown in Fig. 2b).

4.2 Choice of function for fitting

One however desires a more objective way of determining the best misalignments. In principle this can be achieved via a standard (e.g. CURFIT) fitting procedure. One should make a fit and determine the best fit minimizing a chi square (and the confidence intervals from chi square intervals).
A difficulty in this is the choice of the function to be fitted.. What one is actually fitting is a *vector* function or 3 parameters $(x_{fit},y_{fit}) = F(\alpha,\beta,\gamma)(x,y)$ while the CURFIT code is geared onto a scalar function of N parameters A, i.e. $value = F(A_i)(x)$ or even $value = F(A_i)(x,y)$.
However the function itself is strictly used only (via its partial derivatives) to compute the path between one iteration and the next. In order to tell an iteration is better than another one, an estimator is used. This is usually the chi-square defined as follows (where σ_i are customarily the errors on the data instead of the uncertainty on the expectation value):

$$\chi^2 = \sum_i (\mathrm{fit}_i - \mathrm{data}_i)^2/\sigma_i^2$$

but this can easily be replaced by a similar indicator of the same form and interpretation (see next section) based on the fitted and measured (x,y) positions.

In a first instance we have used a standard CURFIT stepping grid, using as (dummy) function x^2-y^2, and the pseudo-chi-square estimator described in the next section.

We have stepped individually each one parameter α,β,γ while the other two were free for fitting (or fixed to a constant value in the case of α). The result was a profile of χ^2 vs the stepped parameter. The best fit was in coincidence of the minimum of the curve and the 90% confidence interval was the one enclosing the values lower than χ^2+2.71 (value for *one* interesting parameter).

This method gives satisfactory results, however one obtains the confidence interval of one parameter at a time, and has to rely on the dummy function with no physical meaning.

4.3 Pseudo-χ^2 estimator

We have therefore resorted to a different method, considering that there are no *uninteresting* parameters in the fit. Either all three misalignment angles are interesting (and one should *step* all of them in a 3-d grid), or α is kept fixed, and the other two angles are stepped on a 2-d grid. This way there is no need of defining a function, or performing a fit (computing partial derivatives). One just *computes* the predicted x_{fit},y_{fit} coordinates for each OP (from the relevant attitude) and *compares* then with the measured x_{meas},y_{meas}.

The comparison can be done via a suitable estimator. The following one is extremely similar to a χ^2 (in fact we have used it also for fitting, see above), but requires the knowledge of an estimate of the error on the measured position(s) σ (we have assumed this error constant for all points).

$$\chi^2 = \sum_i [\, (x_{meas}-x_{fit})^2+(y_{meas}-y_{fit})^2] \,/\, \sigma^2$$

We proceeded as follows : we have produced a map of the denominator of the above formula as a function of β and γ on a 100x100 grid. From this we can later compute a χ^2 for whatever value of σ we choose.
We have produced such grids for a few different values of α within 2 degrees from the "aligned" position (i.e. 0 degrees for M3 and 180 degrees for M1,M2). In fact if we stack such grids on top of each other, we obtain a coarse 3-d grid. The confidence intervals can therefore be obtained using the $\Delta\chi^2$ values relevant to *three* interesting parameters.

4.4 Distance estimator

An alternate and objective estimator (which is independent of the guess of the error σ) is simply the *mean distance* between computed and measured points :

$$d = \left(\sum_i [(x_{meas}-x_{fit})^2+(y_{meas}-y_{fit})^2]^{1/2} \right)/N$$

This distance is computed in mm, but can also be converted in arcsec using the platescale *p=atan(1/1850)* where 1850 mm is the focal length, and provides an intuitive idea of the positioning performance.

We proceeded as follows : contextually to the generation of the above pseudo-chi-square maps we computed also distance maps. The "best fit" based on minimum distance is virtually the same as the one based on minimum chi-square. Confidence contours can be generated for a given maximum mean distance in mm or arcsec.

4.5 Final quality check

The above estimators are used to locate the "best fit" and to assed the errors on the "fitted" parameters. In order to have an impression of the *quality* of the fit (and in particular if there are any bad points) one would like to look at "residuals". One possibility is to compute the residuals as distances in mm, an example of which is shown in fig. 2b. The latter particular case corresponds to a mean distance of 0.085 mm (min 0.009 max 0.22) for LMC X-3 and a mean of 0.24 mm (min 0.09 max 0.78) for Cyg X-1. Note that the largest residuals are for the outermost points, in particular those closest to the calibration sources and to the edge of the Be window.

Another possibility, which gives a more intuitive and helpful view, is to take the measured mm coordinates, and use the attitude and the misalignments to predict the target position on the sky. These coordinates can be compared with the known catalogue position, and plotted as deviation arrows (see fig. 8 and section 5 below)

5 Estimate of misalignment errors

In fig. 3 we report the confidence contours at 68, 90 and 99% for the β and γ angles, obtained in the hypothesis of no rotation around the Z axis (this is α=0 for M3 which has the same orientation of the spacecraft axes, and α=180 for M1 and M2 which are reversed ; note that also the signs of β and γ are also reversed).

In order to compute a chi-square, one need an estimate for the error on the data σ. This has been conservatively assumed constant and equal to 0.17 mm (which is close to one unlinearized pixel).
An example of the effect of reducing s (e.g. to half a pixel, 0.085 mm) is shown in fig. 5a.

The confidence levels are for $\chi^2 = \chi^2_{min} + \Delta\chi^2$ where $\Delta\chi^2$ is the one relevant to three interesting parameters (i.e. 3.5, 6.2 and 11.3 for 68, 90 and 99% confidence).

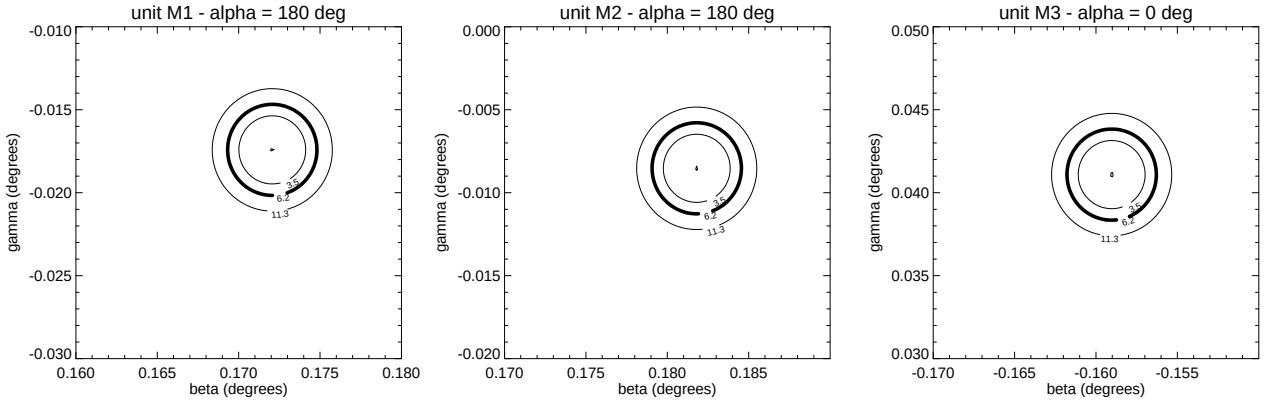

Fig. 3 68, 90 (thick) and 99 % confidence contours for the misalignment angles computed using the chi-square estimator, and assuming σ=0.17 mm. Contours are annotated in $\Delta\chi^2$.

The best fit values and 99% error bars (in degrees) are reported in the table 5.1.

Tab. 5.1

Unit	α	β	γ
M1	180 fixed	0.1722±0.0038	-0.0172±0.0039
M2	180 fixed	0.1820±0.0039	-0.0084±0.0039
M3	0 fixed	-0.1588±0.0039	0.0412±0.0038

The error bars for M3 reduce to 0.0021for β and 0.0020 for γ in the case σ=0.085 (Fig. 5a), i.e. they scale with σ. In search of an objective method to evaluate σ, one can consider the following. One takes the chi-square maps and adjusts σ such that the minimum reduced χ^2 (for 20 degrees of freedom) is equal to unity. In this case one obtains the values in table 5.2.

Tab. 5.2

Unit	error on α	90 and 99% error on β	90 and 99% error on γ	error σ (mm)
M1	fixed	0.0024 0.0033	0.0024 0.0033	0.146
M2	fixed	0.0021 0.0028	0.0021 0.0028	0.122
M3	fixed	0.0019 0.0025	0.0019 0.0025	0.105

In fig. 4 we report an alternate evaluation of the uncertainties on the misalignment, using the mean *distance* between computed and measured points as an estimator. This is independent of the knowledge of the error on the data. In this figure we report contour levels at distances of 0.0448 mm (corresponding to 5 arcsec given the platescale). One can see that the above 90% confidence contours correspond to a distance less than 15 arcsec. The best fit values (in degrees) and the minimum mean distance in mm corresponding to it are reported in the table 5.3. Error bars are at 15 arcsec level.

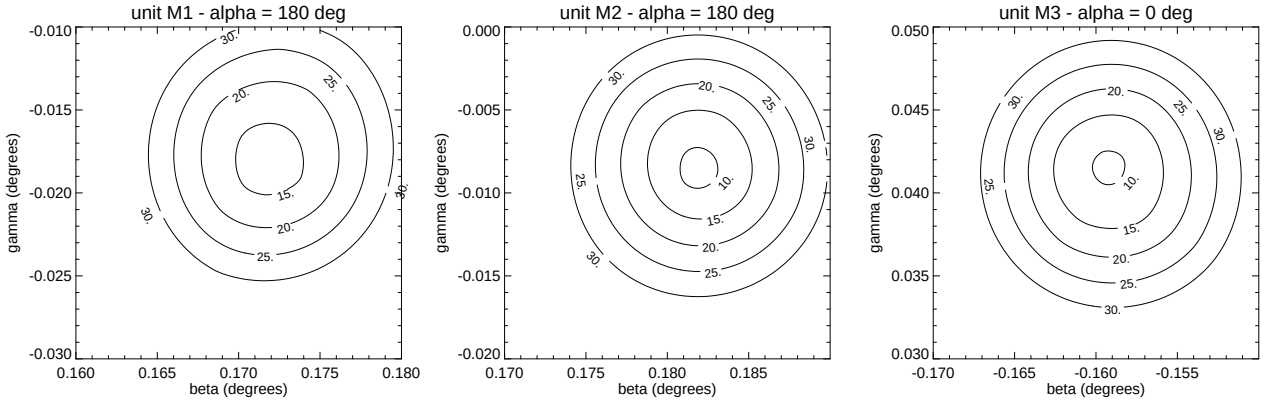

Fig. 4 contours of equal mean distance between predicted and measured positions. Levels are annotated in arcsec and are spaced by 5 arcsec in the range 10 to 30 arcsec.

Tab. 5.3

Unit	α	β	γ	distance (mm)
M1	180 fixed	0.1718±0.0022	-0.0180±0.0021	0.11698
M2	180 fixed	0.1822±0.0022	-0.0084±0.0033	0.07961
M3	0 fixed	-0.1590±0.0036	0.0418±0.0039	0.08445

In both cases the round shape of the contours is indicative of the absence of correlation between the misalignment angles β and γ.

If one considers now the full stack of chi-square or distance maps for different values of α, one can produce contour maps projected onto the βγ plane. One can also construct the envelope of the relevant contour levels, as shown in example (for chi-square and distance respectively) in fig. 5b and 5c.

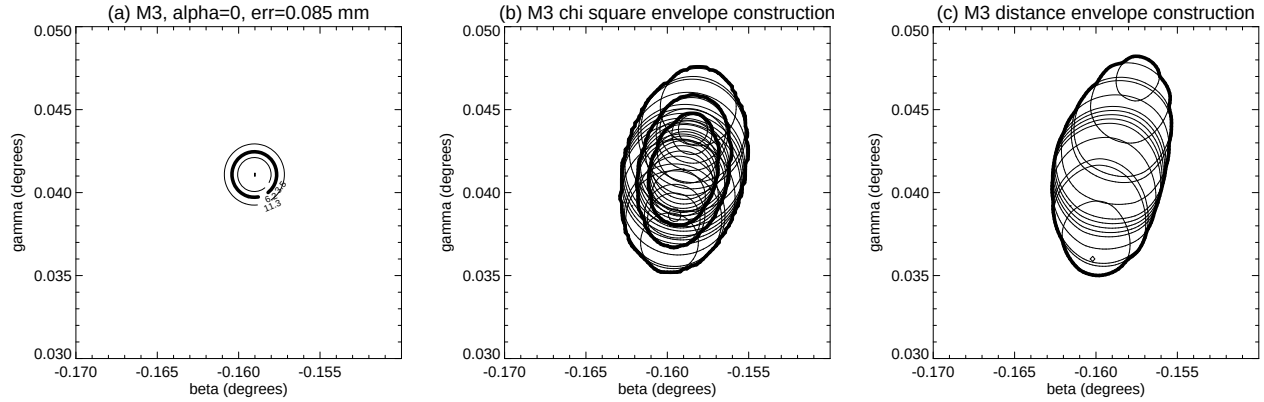

Fig. 5 (a) example of chi-square confidence contours for unit M3 if σ=0.085 mm.
(b) construction of the 68, 90 and 99% confidence contours projected on the βγ plane as envelope of the contours for different values of α (typically ±0.1,0.2,0.5,1.1.5,2 degrees around the aligned value of 0 or 180)
(c) construction of the contours at a distance of 15 projected on the βγ plane as envelope of the contours for the same values of α

In fig. 6 we report the confidence contours obtained by the above method. In the table 5.4 we report the relevant error bars (those on α have been determined manually). The elongation and inclination of the contours indicate some (spurious ?) correlation with the α angle. In table 5.5 we report the errors obtained with the σ values in tab. 5.2 (i.e. forcing minimum chi square to one).

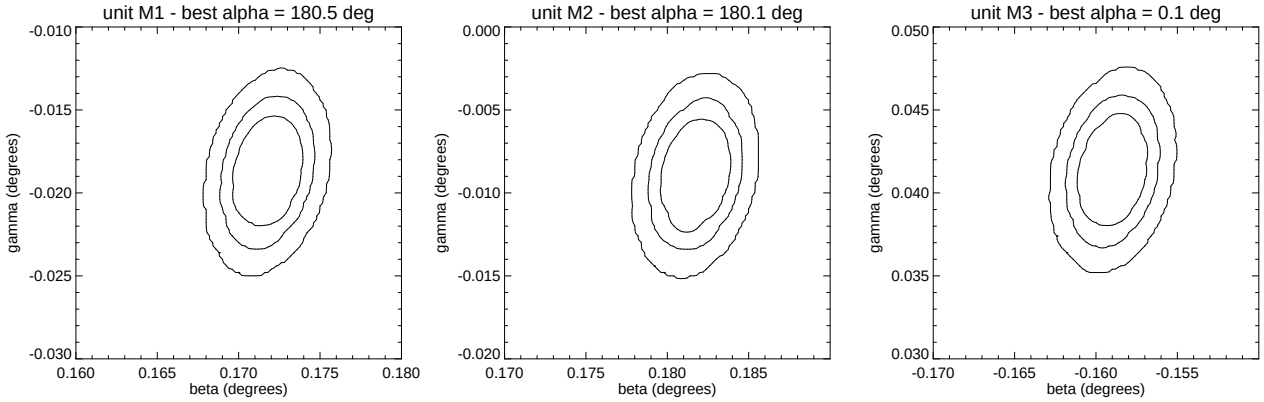

Fig. 6 68, 90 and 99% confidence contours for the misalignment angles β and γ taking into account also the variation with the α angle (see text).

Tab. 5.4

Unit	α	β	γ
M1	180.5±1.5	0.1720±0.0042	-0.0186±0.0064
M2	180.1±1.6	0.1820±0.0042	-0.0086±0.0066
M3	0.1±1.9	-0.1588±0.0041	0.0416±0.0065

Tab. 5.5

Unit	range on α	90 and 99% error on β	90 and 99% error on γ	error σ (mm)
M1	178.5-181.5	0.0027 0.0036	0.0042 0.0054	0.146
M2	178.5-181.5	0.0024 0.0032	0.0036 0.0048	0.122
M3	-0.9 to +0.9	0.0020 0.0026	0.0032 0.0042	0.105

In fig. 7 and in the table 5.6 we report similar results for the distance estimator.

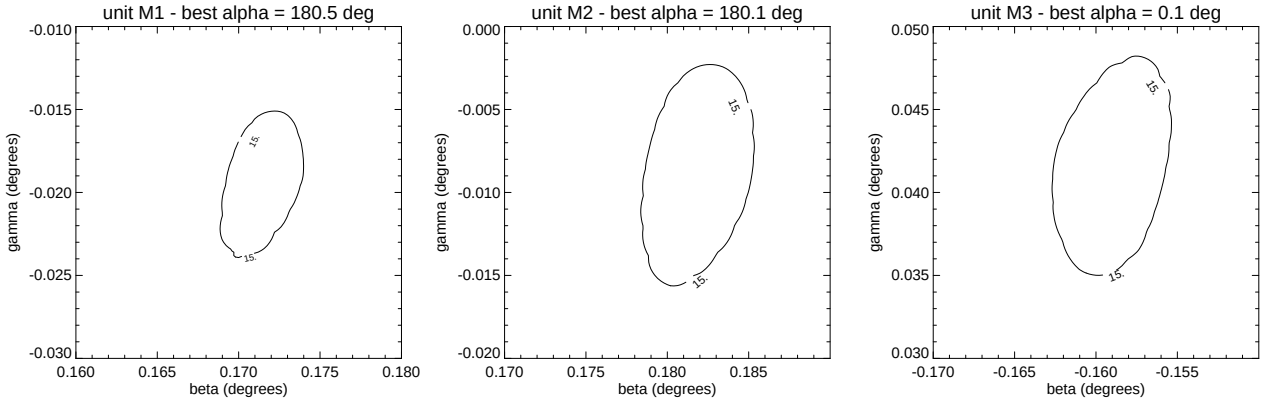

Fig. 7 contours of equal mean distance between predicted and measured, at the level of 15 arcsec, obtained taking into account also the variation with the α angle (see text).

Tab. 5.6

Unit	α	β	γ	distance (mm)
M1	180.5 [179,182]	+0.1714±0.0026	-0.0192±0.0047	0.11431
M2	180.0 [178,182]	+0.1820±0.0037	-0.0088±0.0068	0.07961
M3	0.0 [-2,+2]	-0.1588±0.0039	+0.0420±0.0071	0.08445

In conclusion we have an estimation of the misalignment around the **Z** axis (α) consistent with no rotation within an uncertainty of ±2 degrees, the well known misalignment around the Y axis (β, corresponding to a displacement in the -*x* direction on the image) of 10.4, 10.9 and -9.5 arcmin (for M1,M2 and M3 respectively), and a minor misalignment around the X axis (γ, corresponding to a vertical displacement in the image) of -1.1, -0.5 and +2.5 arcmin respectively, with uncertainties of the order of 0.25 arcmin.

Nominally we can have a choice to use α=0 (or 180), or to take the nominal best fit of α. We have tried both, and the results are quite similar, although marginally better for the perfect alignment around the **Z** axis. *Therefore in the remainder we assume no misalignment around* **Z**.

The effect of the misalignments on the reconstruction of the position are shown in Fig. 8 for data of both LMC X-3 rasters (using the misalignments derived from the same data), and for the Cyg X-1 raster (as control, using the misalignments from the LMC X-3 data).

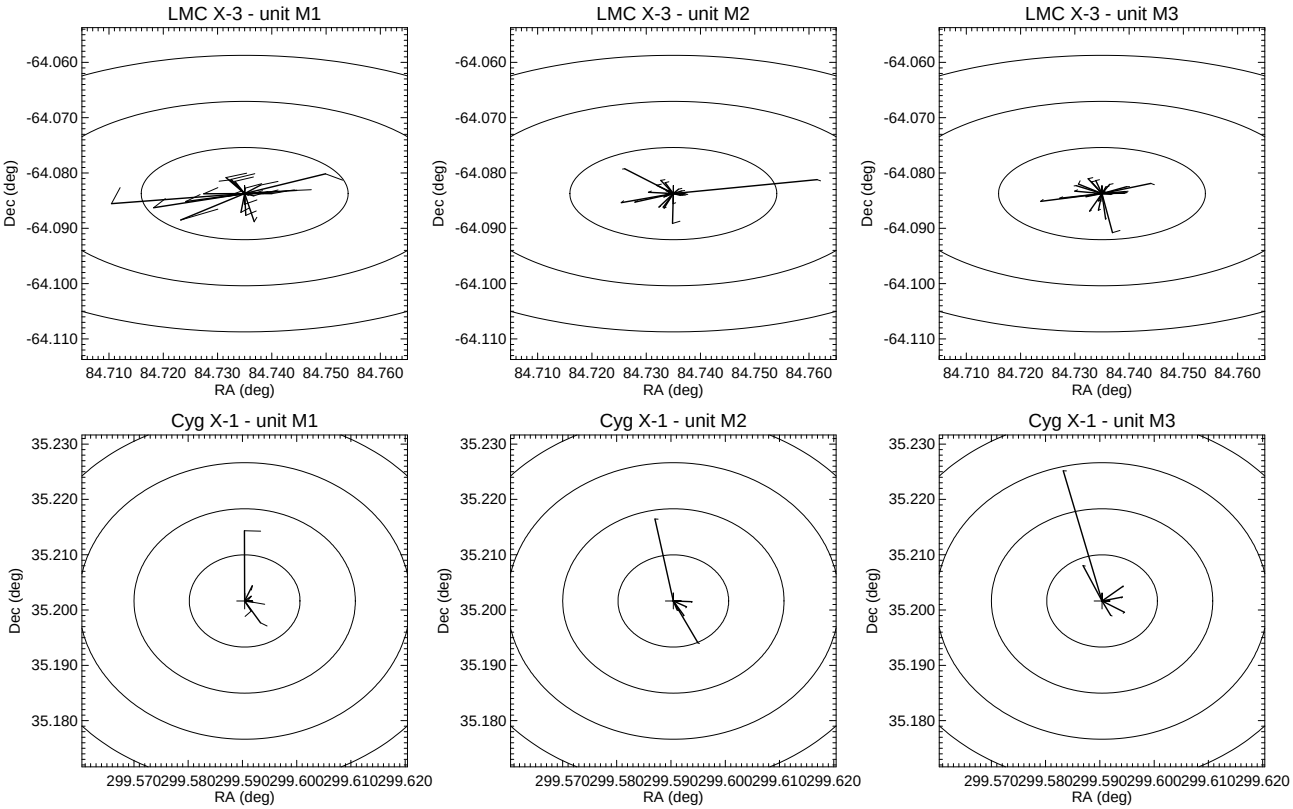

Fig. 8 measured target position is compared to nominal for LMC X-3 and Cyg X-1 rasters. Each frame is ±1.8 arcmin around the catalogue source position. The circles are for an angular distance of 0.5, 1, 1.5 and 2 arcmin. The longer radial segments connect the nominal position with the one measured using no misalignment around **Z** (α=0 or 180), while the shorter tangential segments indicate the effect of introducing a non-zero value of α.

It can be seen that all residuals are well within 30 arcsec (the inner circle) with the exception of the outer points of the first LMC X-3 raster (see Fig. 2a), and of the outermost point of the Cyg X-1 raster. The centroid of most of such points is affected by systematics like the proximity to the calibration sources or the edge of the field of view.

In tables 5.7 and 5.8 we report the mean deviations in arcsec (as angular distances on the sphere) for selected subsets of the data.

Tab. 5.7 : LMC X-3

Unit	All pts	Raster II	Raster I central	Raster I	Raster I outer
M1	13.05	8.59	15.77	19.99	25.25
M2	8.91	5.86	7.58	13.67	21.28
M3	9.47	7.00	12.07	13.32	14.89

Tab. 5.8 : Idem for Cyg X-1 (last point is on very edge)

Unit	All pts	All but last	Last point alone
M1	14.96	8.81	45.7
M2	20.03	13.18	54.25
M3	27.22	15.21	87.31

6 Error budgets

It is desirable to know if there are contributions to positioning errors (on the celestial position of a target measured with the MECS) other than the misalignments, and to make a quantitative breakdown of them. This is attempted below. We have identified three components : the uncertainty on the knowledge of the misalignments, the uncertainty on the attitude, the uncertainty in the pixel centroid determination.

6.1 Evaluation of misalignment error

The uncertainties on the misalignments are described above in section 5.

6.2 Evaluation of attitude error

For what concerns the uncertainty on the attitude we can make the following considerations.
If we limit ourselves to intervals of maximum stability (as done in the misalignment analysis) we see that the variance of the attitude (mean of the time dependent attitude) is within a few arcsec. However the selection of such intervals requires a strong source (is based on a filtering in *xy*), and may severely curtail the length of the intervals used.
If on the other hand one uses less severe constraints (like the intervals where at least 2 star trackers are in use, or even the entire unocculted observation of the target), one is faced with two problems because of sudden jumps in attitude (which are not always in coincidence with star tracker transitions). : the variance around the mean is larger, and the mean is affected by a systematic shift.

Various evaluations of the uncertainty of the attitude are reported in table 6.1. We first have taken the variance of all LMC X-3 at Cyg X-1 attitude profiles used for the misalignment analysis (i.e. at best stability, these are reported in the second column). We have also accumulated a sample (one every other OP for LMC X-3 first raster, and one in 3 OPs for the second raster) of attitude profiles under more relaxed conditions. The column labelled offset indicate the systematic difference in the mean. The typical glitches seen in an attitude time profile are of the order of 30-40 arcsec. Because of their limited length, the mean is offset by a smaller quantity.
The roll angle is a quantity derived from δ_X and δ_Y (formula (6)). Therefore the RA of the X and Y axes is considered uninteresting. The uncertainty on the roll is derived using the error propagation formulae and amounts to a typical value of 1-2 arcmin with spikes up to 15 arcmin.

Tab. 6.1

Interval	max stability	2 STRs		all data	
Quantity q	error σ_q	error σ_q	offset	error σ_q	offset
	all quantities in arcsec				
α_Z	0.5-2.5	9	0 to 2	22	±6
δ_Z	0.2-1.7	6	1	13	0 to 5
α_X	1.5-20	-	-	-	-
δ_X	1-8	8	1	8	0 to 4
α_Y	1-22	-	-	-	-
δ_Y	1-5	7	-2	13	0 to 5

6.3 Evaluation of centroid error

The uncertainty on the determination of the centroid is a function of the algorithm used. Since a selection of possible algorithms (e.g. barycentre, mean or median of PSF or LSF, PSF or LSF fitting) is outside of the scope of the present note, we regard this as an independent variable. In the remainder we will use a parametric value of the order of about one natural detector pixel.

6.4 Method

In order to asses the effects of the various uncertainties, the following general method has been used :

An arbitrary satellite pointing α_Z, δ_Z,ρ has been assumed (exact value).
An arbitrary target position α_T, δ_T has been assumed (typically offset by 0.1 degree and up to 0.4 degrees from the pointing position, which corresponds to typical on- and off-axis observations)
The best misalignments α,β,γ have been used (exact value)
The position of the target in mm (x,y) has been computed
One or more of the quantities α_Z, δ_Z,ρ, α,β,γ, x,y has been perturbed by known amounts consistent with the respective uncertainty range, and a predicted source position α',δ' has been computed.
The perturbation has been repeated for several values
The various α',δ' positions are compared with the known position α_T, δ_T

In practice we have stepped the three misalignments leaving attitude and mm position unperturbed ; we have stepped the attitude using unperturbed misalignments and positions, and we have stepped x,y leaving the remaining quantities unperturbed. An example of the perturbation of an individual parameter for each case is shown in fig. 9. The entire analysis has been done using M3 misalignments. Considered that the amounts and uncertainties on misalignments are similar for the three MECS units this should be representative for all.

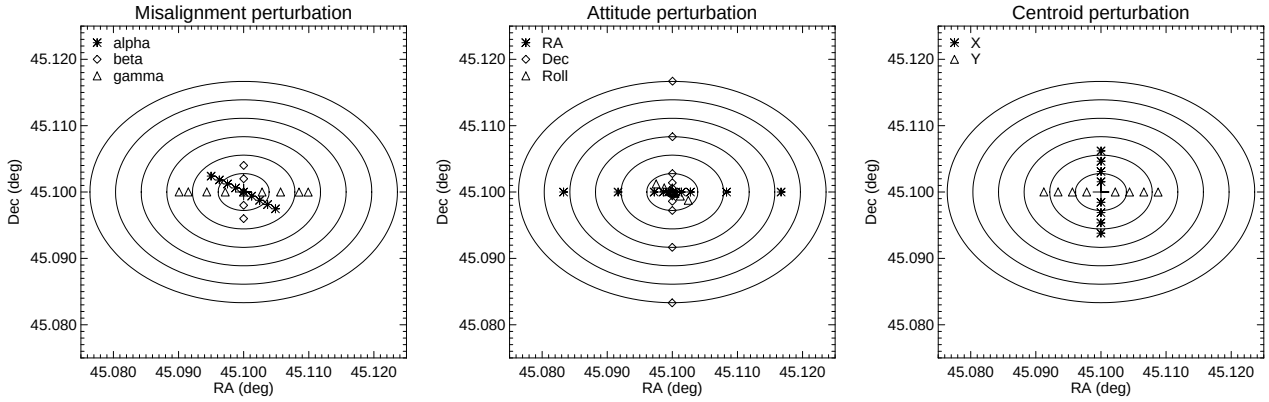

Fig. 9 Panel (a) shows the effect of perturbing the misalignment α by steps of 0.5 degree between ±2 degrees (asterisks), the misalignment β by steps of 0.002 degrees [7 arcsec] around the best value of 10 arcmin (diamonds) and the misalignment γ by steps of 0.002 degrees (with a last step of 0.001) around the best value of 2.5 arcmin (triangles)
Panel (b) shows the effect of perturbing the pointing RA and Dec by ±2,5,10,20,30,60 arcsec (asterisks and diamonds respectively) and the roll angle by ±1,2,5,10,30,60 arcmin (triangles).
Panel (c) shows the effect of perturbing the x,y positions by steps of 0.05 mm between ±0.2 mm.
In all panels the circles show the loci of equal angular distance around the nominal position and are spaced by 10 arcsec up to a maximum of 60 arcsec.

The example has been computed for a pointing at 45,45 degrees, with a roll of 0, and a target at 45.1,45.1 degrees.
A different roll angle ρ will rotate the plot in panel (a) around the centre, with the same range on the reconstructed position. The range of the variation due a perturbation of β is unaffected by a different pointing α_Z, δ_Z. The apparent range covered by the α and γ perturbations increases in the horizontal direction with increasing δ_Z (but the actual angular distance from nominal target remains constant within 25 arcsec max).
The plot in panel (b) is unaffected by variations of the reference α_Z and roll. A perturbation on δ_Z always reflects in a variation of the same amount on the vertical axis, while the effect of a perturbation of α_Z (on the horizontal axes) scales with cos δ_Z.
The plot in panel (c) is obviously unaffected by the the value of the pointing.

6.5 Results

The result of a simultaneous *perturbation of the three misalignments* is show in fig. 10,11 and 12. The values of α,β,γ have been nominally stepped on a 3-d grid between ±2 deg, -0.1628 to -0.1548 deg and 0.0346 to 0.0486 deg respectively. However not all such values are within the formal confidence limits allowed (see section 5). Moreover we have taken a very wide range of γ, which is allowed only for extreme values of α (see e.g. fig. 6). We have therefore flagged the data points using the relevant chi-square maps (see section 5), and do not plot points outside any of the confidence intervals. The following codes apply to all plots. *Thick diamonds* indicate positions allowed by the 90% confidence intervals in Tab. 5.2, and *thick dots* correspond to the 99% interval in the same table. This set of points gives the error box allowed forcing the minimum χ^2 to 1 and assuming α=0 (no misalignment around **Z**). The *triangles* indicate positions allowed by 99% confidence intervals in Tab. 5.1 (i.e. using a more conservative approach on the data error σ, still no misalignment around **Z**). The *asterisks* correspond to the 99% confidence interval of Tab. 5.5 (i.e. minimum χ^2 forced to 1, but allowing the misalignment γ to cover the wider range allowed by a non zero α). The *small dots* are finally the worst case, i.e. the 99% confidence intervals of Tab. 5.4.

Thus the smallest 90% confidence error box is of the order of 10 arcsec, and contained within 20 arcsec for any case assuming no misalignment around **Z**. The effect of a non-null a elongates the error box only if the very conservative choice of σ=0.17 mm is made.

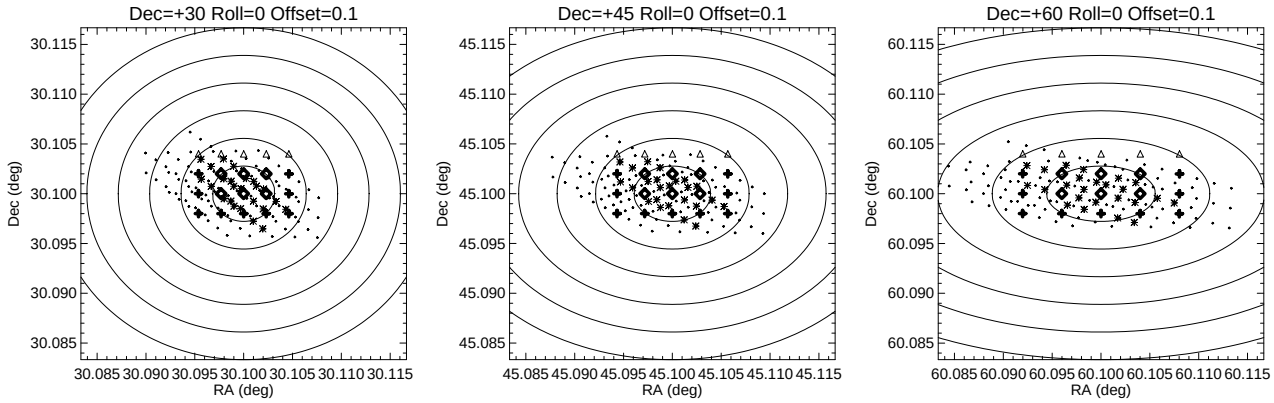

Fig. 10 The symbols (see text) show the predicted source position perturbing the misalignments within their allowed ranges. The different panels correspond to different pointing positions on the sky. The nominal target position is at $\alpha_T=\alpha_Z+\Delta$, $\delta_T=\delta_Z+\Delta$, where the offset Δ in degree is given for each panel. In all panels the circles show the loci of equal angular distance around the nominal position and are spaced by 10 arcsec up to a maximum of 60 arcsec

Figures 11 and 12 show respectively the effect of varying the roll angle, and of different off-axis positions (the cases shown with offsets of 0.1, 0.2, 0.3 and 0.4 degrees correspond to 2.5, 5, 9 and 13 mm from detector centre). Note that the elongation of the error box with the off-axis angle increases only if one considers a non-null misalignment around the **Z** axis.

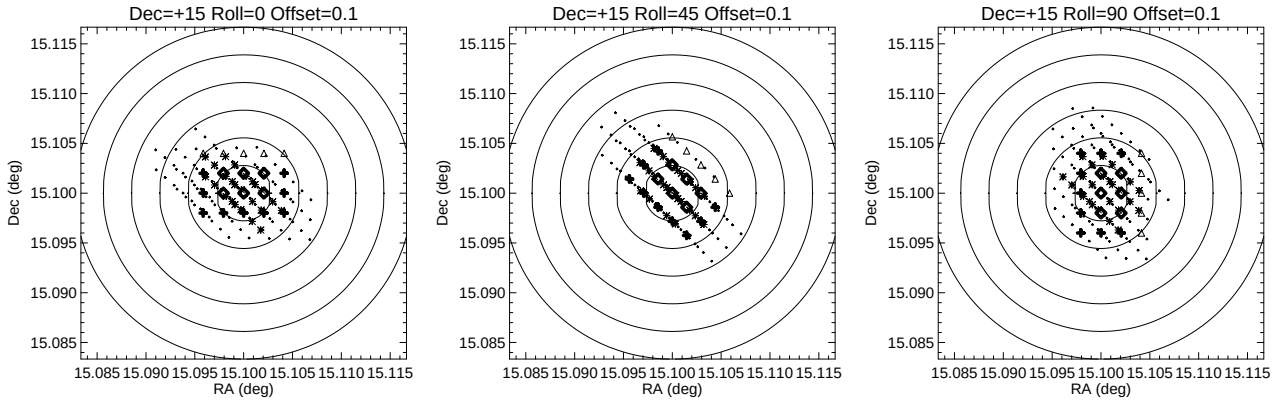

Fig. 11 The symbols (see text) show the predicted source position perturbing the misalignments within their allowed ranges. The different panels correspond to different roll angles for the same pointing direction.

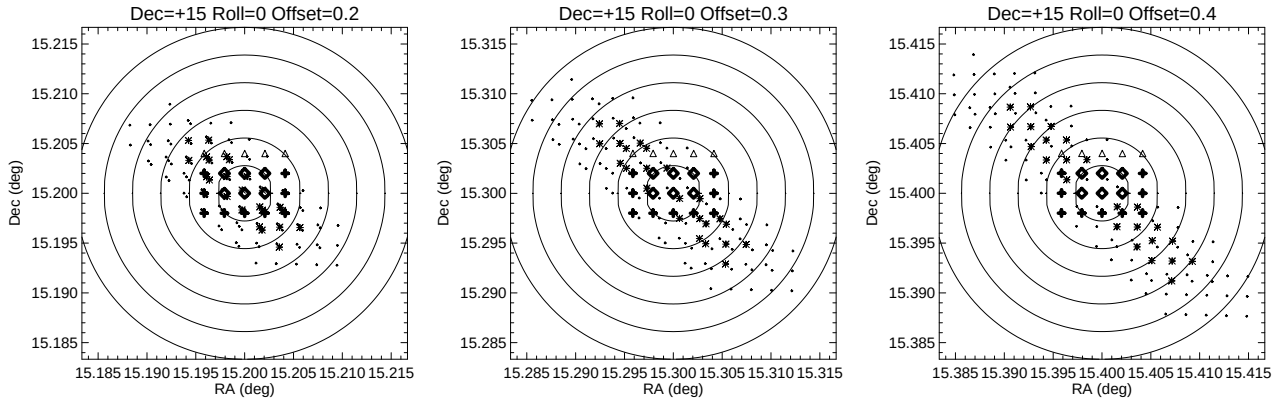

Fig. 12 The symbols(see text) show the predicted source position perturbing the misalignments within their allowed ranges. The different panels correspond to different target positions at $\alpha_T=\alpha_Z+\Delta$, $\delta_T=\delta_Z+\Delta$, where the offset Δ in degree is given for each panel for the same pointing direction $(\alpha_Z, \delta_Z) = (15,15)$.

The result of a simultaneous *perturbation of the pointing direction* is shown in fig. 13. The values of the pointing RA and Dec have been stepped by ±10,20,30 arcsec, while the roll angle by ±10,20,30 arcmin. It can clearly be seen that the effect of an uncertainty on the roll angle is small, while the effect of an uncertainty on RA and Dec reflects on an equal error on the predicted position (the error on RA is of course reduced by a factor cosδ).

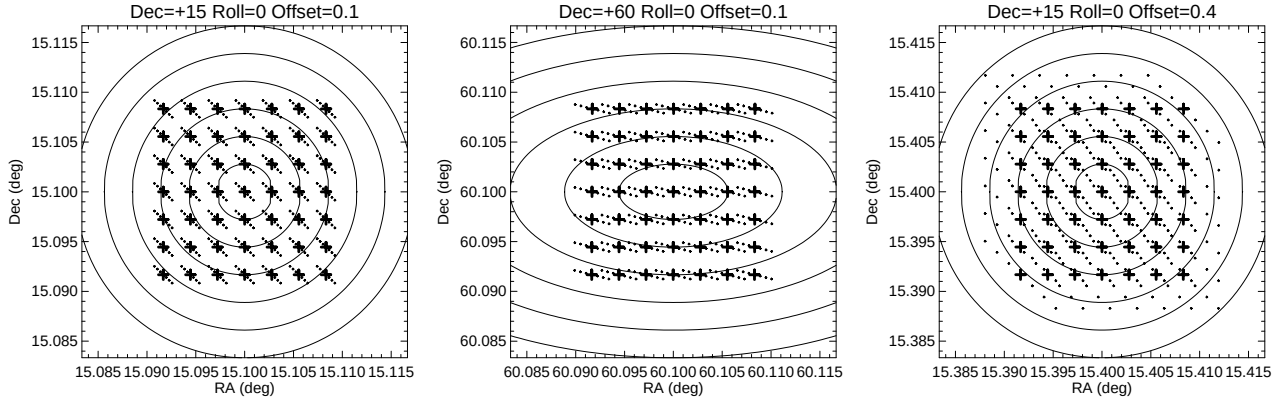

Fig. 13 The symbols show the predicted source position perturbing the pointing direction within the ranges given in the text. The different panels correspond to different declinations and/or off-axis angles. The thick crosses indicate the values for zero roll angle. Each cross has an oblique row of dots associated with it in correspondence of the different roll angles.

The result of a *perturbation of the measured target position in mm* is not shown, since it obviously scales with the platescale. A linear displacement of 0.2 mm (the maximum we have considered) corresponds to about 25 arcsec.

The result of a worst case combination of all errors is shown in fig. 14. In this case we have assumed the α misalignment to be exactly zero with no error, and we have also neglected the roll angle errors. For the remaining quantities we have stepped each of them just of a single step above and below the reference value, and namely : α_Z and δ_Z have been stepped by ±30 arcsec, the mm positions *x* and *y* by ±0.2 mm, the misalignment β by ±0.002 deg and the misalignment γ by ±0.004 deg. Note that all ranges are conservatively taken rather wide.

The resulting range of about one arcmin matches well with the combination of the different uncertainties with the usual sum of squares rule.

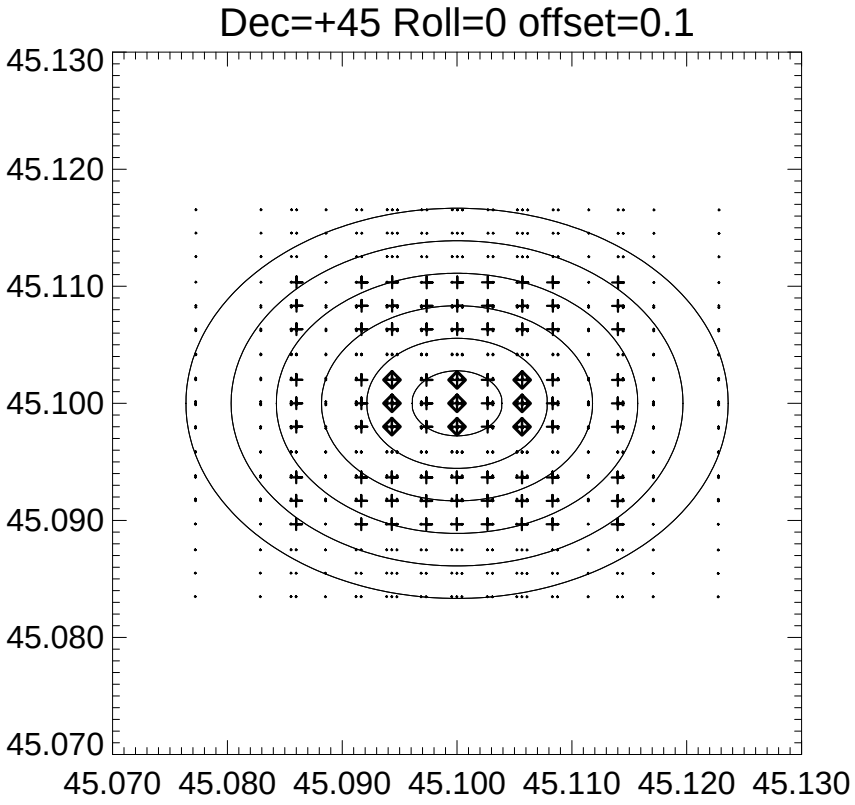

Fig. 14 The symbols show the predicted source position perturbing the misalignments, pointing direction and measured positions given in the text..The group of 9 diamonds at the centre indicate the effect of the uncertainty on the misalignments alone. This group of 9 points is moved around (up, down, right, left) according to an uncertainty of 30 arcsec on pointing direction, as shown by the crosses. The dots show the effect of introducing a further perturbation of 0.2 mm on the measured centroid.

A Appendix : Notation and mathematics

We summarize here the various formulae used in the misalignment analysis and related software

A.1 Euler angles - definition

Any rotation can be described by *three* angles. In particular the satellite attitude can be described as a rotation w.r.t. to the celestial (equatorial) coordinate system, or the detector misalignments can be described as a rotation w.r.t. the satellite coordinate system. We follow here the notation for Euler angles used by Goldstein (*Classical Mechanics*). The three angles are called ϕ,θ,ψ and the rotations are defined strictly in the following way and order :

One first rotates xyz into x' y' z' around axis z by angle ϕ
One than rotates (inclinates) x' y' z' into x"y"z" around axis x' by angle θ
One finally rotates x"y"z" into the final position around axis z" by angle ψ.

The transformation matrix is written in the form (1)

$$\begin{bmatrix} \cos\psi\cos\phi-\cos\theta\sin\phi\sin\psi & \cos\psi\sin\phi+\cos\theta\cos\phi\sin\psi & \sin\psi\sin\theta \\ -\sin\psi\cos\phi-\cos\theta\sin\phi\cos\psi & -\sin\psi\sin\phi+\cos\theta\cos\phi\cos\psi & \cos\psi\sin\theta \\ \sin\theta\sin\phi & -\sin\theta\cos\phi & \cos\theta \end{bmatrix}$$

A.2 Attitude definition

The satellite *attitude* is described by the orientation of the spacecraft axes **XYZ** with respect to the celestial sphere axes **xyz**. It can be formally described as a rotation (see A.4).
It is available in the attitude file as 6 angles, i.e. the (α,δ) of each of the axes **XYZ** in the system **xyz**. These angles (which are of course not all independent) will be indicated as

$(\alpha_X,\delta_X)\,(\alpha_Y,\delta_Y)\,(\alpha_Z,\delta_Z)$

A.3 Celestial to cartesian coordinate conversion and v.v.

i Celestial to cartesian

Given the celestial coordinates of a point on the unitary sphere, its cartesian coordinates can be computed as :

$$\begin{aligned} \mathbf{x} &= \cos\delta\cos\alpha \\ \mathbf{y} &= \cos\delta\sin\alpha \\ \mathbf{z} &= \sin\delta \end{aligned} \qquad (2)$$

ii Cartesian to celestial

The inverse relationship which gives the celestial coordinates given the cartesian coordinates on the unitary sphere is :

$$\begin{aligned} \alpha &= \mathrm{atan}\,(\mathbf{x}/\mathbf{y}) \\ \delta &= \mathrm{atan}\,(\,\mathbf{z}\,/(\mathbf{x}^2+\mathbf{y}^2)^{1/2}\,) \end{aligned} \qquad (3)$$

A.4 Euler angle (attitude) matrix - computation

Given the 6 angular coordinates of the three satellite axes $(\alpha_X,\delta_X),(\alpha_Y,\delta_Y),(\alpha_Z,\delta_Z)$ one can compute the **x**,**y**,**z** components of the rotated axes using either Euler angles in formula (1), or using the celestial to cartesian conversion (formulae (2), which provide an alternate method to fill in the Euler matrix) :

$$
\begin{aligned}
x_X &= \cos\psi\cos\phi-\cos\theta\sin\phi\sin\psi = \cos\delta_X\cos\alpha_X \\
y_X &= \cos\psi\sin\phi+\cos\theta\cos\phi\sin\psi = \cos\delta_X\sin\alpha_X \qquad (4a)\\
z_X &= \sin\psi\sin\theta = \sin\delta_X \\
x_Y &= -\sin\psi\cos\phi-\cos\theta\sin\phi\cos\psi = \cos\delta_Y\cos\alpha_Y \\
y_Y &= -\sin\psi\sin\phi+\cos\theta\cos\phi\cos\psi = \cos\delta_Y\sin\alpha_Y \qquad (4b)\\
z_Y &= \cos\psi\sin\theta = \sin\delta_Y \\
x_Z &= \sin\theta\sin\phi = \cos\delta_Z\cos\alpha_Z \\
y_Z &= -\sin\theta\cos\phi = \cos\delta_Z\sin\alpha_Z \qquad (4c)\\
z_Z &= \cos\theta = \sin\delta_Z
\end{aligned}
$$

The form used in the software to construct the satellite attitude (Euler) matrix requires the knowledge of the Euler angles, which are related to the pointing and roll angle by relations :

$$\theta = 90-\delta_Z \qquad (5a)$$

$$\phi = 90+\alpha_Z \qquad (5b)$$

$$\psi=90-\rho \qquad (5c)$$

In practice angle ψ is computed using the following formula (one of several equivalent ones).

$$\tan\psi = z_X/z_Y = \sin\delta_X/\sin\delta_Y \qquad (6)$$

A.5 Misalignment matrix

For what concerns the misalignments (see also fig. 1), instead of the Euler angles we have used the rotations around the three axes, which are more intuitive.The misalignment matrix is given composing the rotation around the three axes **Z**,**Y**,**X** by angles $\alpha\ \beta\ \gamma$ in the quoted order of application, i.e. the matrix A_{mis} is

$$
\begin{bmatrix} 1 & 0 & 0 \\ 0 & \cos\gamma & \sin\gamma \\ 0 & -\sin\gamma & \cos\gamma \end{bmatrix}
\begin{bmatrix} \cos\beta & 0 & \sin\beta \\ 0 & 1 & 0 \\ -\sin\beta & 0 & \cos\beta \end{bmatrix}
\begin{bmatrix} \cos\alpha & \sin\alpha & 0 \\ -\sin\alpha & \cos\alpha & 0 \\ 0 & 0 & 1 \end{bmatrix} \qquad (7)
$$

A.6 Modified (detector) attitude matrix

The detector attitude can therefore be derived in form of an Euler matrix, multiplying the spacecraft Euler matrix by the misalignment matrix as

$$E_{det}=A_{mis}E_{s/c} \qquad (8)$$

A.7 Gnomonic coordinates - definition

According to Murray (*Vectorial astrometry*) the "standard coordinates" in the tangential plane can be computed as follows. One considers the vectors of three pointing axes (e.g. the **Z** axis and the two "natural" orthogonal axes, in which case α,δ are α_Z, δ_Z) and gives them the following names :

$$\begin{aligned} \mathbf{u} &= [x_P,y_P,z_P] = & [-\sin\alpha, & \cos\alpha, & 0] \\ \mathbf{v} &= [x_Q,y_Q,z_Q] = & [-\sin\delta\cos\alpha, & -\sin\delta\sin\alpha, & \cos\delta] \\ \mathbf{w} &= [x_Z,y_Z,z_Z] = & [\cos\delta\cos\alpha, & \cos\delta\sin\alpha, & \sin\delta] \end{aligned} \qquad (9)$$

One also considers the vector **R** corresponding to the target position

$$\mathbf{R} = [x_T,y_T,z_T] = [\cos\delta_T\cos\alpha_T, \quad \cos\delta_T\sin\alpha_T, \quad \sin\delta_T] \qquad (10)$$

And considers their dot products **u**·**R**, **v**·**R**, and **w**·**R** and defines the "standard coordinates" as

$$\begin{aligned} \xi &= \mathbf{u}\cdot\mathbf{R}/\mathbf{w}\cdot\mathbf{R} \\ \eta &= \mathbf{v}\cdot\mathbf{R}/\mathbf{w}\cdot\mathbf{R} \end{aligned} \qquad (11)$$

Note that these coordinates are angular coordinates and have a default orientation on the sky.

A.8 Gnomonic coordinates - application

For what concerns SAX, the detector coordinates *x y* in mm can be derived by the gnomonic coordinates (11) by a 90 degree axis exchange, and a rotation by the opposite of the detector roll angle (see A.11.iii), plus the conversion from angular to linear using the platescale :

$$p = \text{atan}\,(1/1850) \qquad (12)$$

$$\begin{aligned} \xi' &= \eta \\ \eta' &= -\xi \\ \rho' &= -\rho \end{aligned} \qquad (13)$$

$$\begin{aligned} x &= -(\xi' \cos\rho' + \eta' \sin\rho')/p \\ y &= -(-\xi' \sin\rho' + \eta' \cos\rho')/p \end{aligned} \qquad (14)$$

One can combine definitions (13) with formulae (14) using ρ as the roll angle (remember the parities of cos and sin) :

$$\begin{aligned} x &= -(\eta\cos\rho + \xi\sin\rho)/p \\ y &= (-\eta\sin\rho + \xi\cos\rho)/p \end{aligned} \qquad (15)$$

A.9 Alternate derivation

The following formulae are used by SAXDAS. They offer a way to derive the *x,y* directly in the detector orientation without explicit use of the roll, but at the expense of a second angular conversion. We have verified these formulae give the same result as formulae (15) which are the ones used for misalignment analysis.

The target position is defined by the same vector **R** defined in formula (10)

One can then define three vectors corresponding to the cartesian coordinates of the axes. For null roll angle, and given the attitude Euler matrix for the spacecraft, these vectors are the same as the **u v w** defined in formula (9) above. For a generic Euler matrix N, eventually misaligned, one has that such vectors are given by :

$$\begin{aligned} \mathbf{u}' &= [x_X,y_X,z_X] = & [N_{11}\ N_{12}\ N_{13}] \\ \mathbf{v}' &= [x_Y,y_Y,z_Y] = & [N_{21}\ N_{22}\ N_{23}] \\ \mathbf{w}' &= [x_Z,y_Z,z_Z] = & [N_{31}\ N_{32}\ N_{33}] \end{aligned} \qquad (16)$$

One can then define the three scalar products :

$$V_1 = \mathbf{u'}\cdot\mathbf{R}$$
$$V_2 = \mathbf{v'}\cdot\mathbf{R} \quad (17)$$
$$V_3 = \mathbf{w'}\cdot\mathbf{R}$$

and then take from these two angular quantities :

$$\tau = \text{acos}\,(V_3) \quad (18)$$
$$\sigma = \text{atan}\,(V_2/V_1)$$

and define the *xy* coordinates as follows (the minus sign gives coordinates already in the orientation for M3 while the platescale (12) is applied to convert to mm) :

$$x = -\tau\cos\sigma/p \quad (19)$$
$$y = -\tau\,\sin\sigma/p$$

A.10 Linearization

The linearization relates raw (electronics) coordinates to physical detector coordinates. A full description is outside of the scope of the present note. We remind only the basic formulae.

i from raw pixels to mm

The raw x_u,y_u position of a photon is converted to mm on the detector surface (with origin at the centre as determined by the strongback) using the linearization coefficients A_1.. A_{10} (and the photon energy in keV) :

$$x'_u = x_u - A_1 \quad (20)$$
$$y'_u = y_u - A_2$$

Formula (20) gives coordinates in raw pixels relative to the centre of the detector (A_1, A_2). Formula (21) converts them to mm (with the detector centre being *x*,*y*=(0,0) mm).

$$x = A_3\,(1+A_7/E)\,x'_u + A_5\,x'^2_u + A_9\,x'^3_u \quad (21)$$
$$y = A_4\,(1+A_8/E)\,x'_u + A_6\,y'^2_u + A_{10}\,y'^3_u$$

This first step is sufficient for the misalignment analysis. The application of the first step for event linearization includes additional ±0.5 pixel randomization and post facto integer conversion, which are ignored here.

ii from mm to linearized pixels

Usually however(e.g. when accumulating an image) one wants to perform a second step to project mm positions onto "new" pixels x_l,y_l of arbitrary size Δ. This second step requires a choice of a new centre. The common definition uses the resulting linearized coordinates of the centre (which are (128,128) if the pixels size is the "natural" one, i.e. the size of an unlinearized pixel at the centre i.e $(A_3+ A_4)/2$) such that the entire field of view is covered. The term *h* is computed internally by the correction routines.

$$h = \text{centre}\;\Delta = 128\;\Delta_{natural} \quad (22)$$
$$x_l = (x+h)/\Delta \quad (23)$$
$$y_l = (y+h)/\Delta$$

iii from linearized pixels to mm

If one has positions already in linearized pixels x_l,y_l one can derive the mm coordinates computing from (23) the centre of the detector in linearized pixels of size Δ, with the term *h* from formula (23).

$$x_c = (0+h)/\Delta \qquad (24)$$
$$y_c = (0+h)/\Delta$$

and inverting the (22). These coordinates have detector orientation (i.e. M1 and M2 are opposite to M3 and to the spacecraft - the inversion is later taken care by the appropriate definition of the misalignment)

$$x = (x_l - x_c)\Delta \qquad (25)$$
$$y = (y_l - y_c)\Delta$$

A.11 Celestial to detector coordinate conversion and v.v.

i Celestial to detector

In order to convert a target celestial coordinate α_T,δ_T to detector coordinates *x*,*y* one need to know the satellite attitude (α_Z δ_Z ρ) and the misalignments.

One uses formulae (5) and (4) to construct the satellite Euler matrix.
One uses formula (7) to build the misalignment matrix.
One computes the detector Euler matrix with formula (8)
One uses formula (28) below to determine the detector attitude (α_D δ_D ρ_D).
One uses formulae (9) to (14) to compute standard gnomonic coordinates (using as α,δ,ρ the above detector attitude) and to convert them to mm on the detector plane *x y*.
If one desires linearized pixels, one shall apply also formulae (22) and (23)

ii Detector to celestial

The inverse conversion from measured detector coordinates to the relevant celestial coordinates passes through the following steps (however one still needs to know the satellite attitude (α_Z δ_Z ρ) and the misalignments) :

If not already available one converts pixels to mm using formulae (24-25)
One uses formulae (5) and (4) to construct the satellite Euler matrix.
One uses formula (7) to build the misalignment matrix.
One computes the detector Euler matrix with formula (8)
One uses formula (28) below to determine the detector attitude (α_D δ_D ρ_D).
One convert from mm to angular using the platescale (12), inverting formulae (13) and derotating by the detector roll angle ρ_D as follows :

$$\xi' = yp$$
$$\eta' = xp \qquad (26)$$
$$\rho' = -\rho_D$$
$$\xi = \xi' \cos\rho' + \eta' \sin\rho' \qquad (27)$$
$$\eta = \xi' \sin\rho' - \eta' \cos\rho'$$

One inverts the gnomonic coordinates using formulae (29), using as pointing coordinates the detector attitude.

iii from Euler matrix to attitude celestial coordinates

Given an Euler matrix M (be it spacecraft or detector) of the following form (with the Fortran storage order as given) :

$$\begin{bmatrix} M_{11} & M_{12} & M_{13} \end{bmatrix} \qquad \begin{bmatrix} 1 & 4 & 7 \end{bmatrix}$$

$$\begin{vmatrix} M_{21} & M_{22} & M_{23} \\ M_{31} & M_{32} & M_{33} \end{vmatrix} \quad \begin{vmatrix} 2 & 5 & 8 \\ 3 & 6 & 9 \end{vmatrix}$$

one obtains the associated attitude (the subscript P may be replaced by Z for spacecraft or D for detector) as follows (similar formulae hold for the other two axes) :

$$\begin{aligned} \alpha_P &= \text{atan}\,(M_{32}/M_{31}) \\ \delta_P &= \text{asin}\,(M_{33}) \\ \rho_P &= \text{atan}\,[M_{23}/(M_{21}M_{32} - M_{22}M_{31})] \end{aligned} \qquad (28)$$

iv from gnomonic to celestial coordinates

The following formulae are taken from the *Exosat Observers' Guide Part III*. The above formulae (26) and (27) are necessary to adjust the SAX coordinate convention to the Exosat one. Here α_P, δ_P are the pointing coordinates (spacecraft Z or detector D), and α,δ is the resulting celestial position.

The inversion of gnomonic coordinates is not straightforward, but can be obtained by :

$$\begin{aligned} r^2 &= \xi^2 + \eta^2 \\ A &= \sin\delta = \cos r \sin\delta_P + \eta\cos\delta_P \sin r / r \\ B &= \cos\delta \text{ such that } B^2 = 1 - A^2 \\ \delta &= \text{atan}\,(A/B) \end{aligned} \qquad (29a)$$

$$\begin{aligned} C &= \sin\Delta\alpha = (\sin r / r)\ (\xi/\cos\delta) \\ D &= \cos\Delta\alpha = (\cos r \cos\delta_P - \eta\sin\delta_P \sin r / r) / \cos\delta \\ \Delta\alpha &= \text{atan}\,(C/D) \\ \alpha &= \alpha_P + \Delta\alpha \end{aligned} \qquad (29b)$$

with two singular cases which must be treated differently :

if r=0	by definition	$\alpha=\alpha_P$	$\delta=\delta_P$
if B=0		$\alpha=\alpha_P$	$\delta=\pm 90$ according to the sign of δ_P

A.12 aberrare humanum est ?

The positions in the attitude files (see A.2) are "referred to the mean of date 2000" (*FOT Layout Document*), therefore they are "mean places" according to the definition in the Glossary of the *Astronomical Almanac*, which means that several effects (of which the only relevant one is *annual aberration*) have been removed.

For a non-planetary object the "mean place" and the "geometric place" are the same, and the correction for aberration at pag. B17 of the *Astronomical Almanac* leads to the "apparent geocentric place".

i Annual aberration - definitions

The apparent geocentric place α,δ is derived from the geometric α_0,δ_0 via :

$$\alpha=\alpha_0+\Delta\alpha \qquad (30)$$
$$\delta=\delta_0+\Delta\delta$$

The difference in coordinates are given by :

$$\Delta\alpha = (-v_x \sin\alpha_0 + v_y \cos\alpha_0)/ (c \cos\delta_0) \qquad (31)$$
$$\Delta\delta = (-v_x \cos\alpha_0 \sin\delta_0 - v_y \sin\alpha_0 \sin\delta_0 + v_z \cos\delta_0) c$$

with c =173.14 AU/day. If the aberration constant (pag. K6 of the *Astronomical Almanac*) is κ=20.49552 arcsec, the components of the velocity of the Sun are given by

$$vx = c\kappa\sin\lambda$$
$$vy = -c\kappa\cos\varepsilon\cos\lambda \qquad (32)$$
$$vz = -c\kappa\sin\varepsilon\cos\lambda$$

and the ecliptic coordinates ε,λ are given as a function of time (in practice only the longitude λ can be assumed variable) in degrees as

$$\lambda = L+1.915 \sin g + 0.020 \sin 2g \qquad (33)$$
$$\varepsilon = 23.439 - 0.0000004\ n$$

with terms L and g (normalized modulo 0-360) given (also in degrees) by

$$L = 280.460 + 0.9856474\ n \qquad (34)$$
$$g = 357.528 + 0.9856003\ n$$

and n is related to the time t (in days) since beginning of the year 1993

$$n = -2557.5 + t = JD -2451545.0 \qquad (35)$$

ii Applicability

Are measured target positions to be considered "apparent geocentric places" ?
And what about catalog positions ?
Should one apply aberration to all/some of them in order to be consistent with the SAX attitude files ?

The aberration for LMC X-3 varies between $\Delta\alpha$ = 5.5 arcsec (first raster) and 6.5 arcsec (second raster), with $\Delta\delta$ = 20.4 arcsec for both epochs.

We have tried the misalignment analysis using spacecraft attitude and catalogue positions as available (unaberrated) and also correcting *both* for aberration. Since there was no difference on the computed misalignments, we have neglected aberration for this analysis (but is this the correct way for data reduction ?).